Original article

PARAMETER STUDY AND OPTIMIZATION OF AN AMPEROMETRIC BIOSENSOR FOR PYRUVATE DETERMINATION USING MATHEMATICAL MODELING

Y.V. Karpenko [1]*, O.O. Soldatkin [1,2], N. Jaffrezic-Renault [3]

[1]Institute of Molecular Biology and Genetics, NAS of Ukraine, Kyiv, Ukraine
[2]Igor Sikorsky Kyiv Polytechnic Institute, Kyiv, Ukraine
[3]Institute of Analytical Sciences, University of Lyon, Villeurbanne, France

*Corresponding author: ukr.karpenko.yu@gmail.com

Background. Pyruvate serves as an important diagnostic marker of mitochondrial dysfunctions, lactic acidosis, and certain oncological diseases. Traditional methods for pyruvate analysis have a number of significant limitations: they require complex equipment, are labor-intensive, involve time-consuming sample preparation. Therefore, the development of new, sensitive, and selective methods for determining pyruvate concentration is a highly relevant task.

Objective. The aim of this work was to develop a procedure for the determination and optimization of the parameters of a mathematical model of an amperometric biosensor based on immobilized pyruvate oxidase, employing mathematical modeling of diffusion–reaction processes.

Methods. The biosensor was fabricated using a photopolymer matrix. The analytical characteristics of the biosensor were investigated experimentally. Reaction–diffusion mathematical model was developed to analyze the sensitivity of the biosensor to the substrate (pyruvate) with respect to system parameters. Optimization of these parameters was performed using the gradient descent method.

Results. The study demonstrated that the pyruvate oxidase-based biosensor exhibited a stable amperometric response to pyruvate. Model analysis revealed a significant influence of the substrate diffusion coefficient and the thickness of the bioselective membrane on the biosensor's sensitivity to pyruvate. The responses of the biosensors showed high signal reproducibility. The theoretically calculated response curves of the biosensor were in good agreement with the experimental data.

Conclusions. The biosensor is characterized by high sensitivity and reproducibility in pyruvate determination. Mathematical modeling enabled rational optimization of the biosensor parameters. The influence of all parameters on the biosensor sensitivity decreased in the following order: from the most influential enzymatic reaction rate constant (k), to the substrate diffusion coefficient (D_S), to the membrane thickness (L), whereas the effect of the product diffusion coefficient (D_P) was found to be minimal.

Keywords: pyruvate; amperometric biosensor; pyruvate oxidase; reaction-diffusion model; optimization

Introduction

Pyruvate (pyruvic acid) is a key intermediate metabolite in cellular energy metabolism, particularly in glycolysis, gluconeogenesis, and the tricarboxylic acid cycle [1]. Its concentration in biological fluids serves as an important diagnostic marker associated with metabolic disorders, including lactic acidosis, mitochondrial dysfunctions, and certain oncological diseases [2, 3]. Therefore, the development of highly sensitive, selective, and rapid methods for pyruvate determination remains a relevant challenge in analytical biochemistry and medical diagnostics.

Traditional methods for pyruvate analysis, such as spectrophotometric, fluorometric, and chromatographic approaches, are widely employed in biochemical studies and clinical diagnostics. However, these techniques exhibit several critical limitations: they require complex and expensive instrumentation, are labor-intensive, involve time-consuming sample preparation, and often necessitate additional reagents as well as multistep procedures. Consequently, such methods are not always suitable for real-time monitoring of metabolite concentrations or for integration into portable diagnostic platforms. These constraints underscore the importance of developing novel sensing technologies that combine high sensitivity and selectivity with operational simplicity.

Among the available methods for pyruvate detection, amperometric biosensors have gained considerable attention due to their high sensitivity, ease of operation, potential for miniaturization, and compatibility with portable diagnostic devices [4], advantages that are difficult to achieve with conventional analytical techniques for pyruvate quantification. Biosensors based on the enzyme pyruvate oxidase (EC 1.2.3.3) enable selective conversion of pyruvate into acetate and hydrogen peroxide, the latter being further de-

tected by amperometric methods [5]. This strategy facilitates direct electrochemical monitoring of pyruvate concentrations in real time.

In recent years, substantial progress has been achieved in immobilization strategies for pyruvate oxidase (POx) on transducer surfaces, employing nanomaterials, polymers, and hybrid matrices to enhance enzyme stability, electron transfer, and catalytic efficiency [6, 7]. Research efforts have also focused on optimizing the enzyme's operating conditions, including pH, temperature, and the presence of cofactors (e.g., *FAD*, *TPP*, Mg^{2+}), all of which play a critical role in biosensor performance [8].

An essential component of modern biosensor development is mathematical modeling of enzymatic reaction kinetics, substrate diffusion, and signal generation. Modeling enables prediction of biosensor behavior under various conditions, rational optimization of sensor design, and interpretation of experimental results without the need for extensive trial-and-error experimentation. A significant contribution to this field has been made by the group of Baronas, who proposed a series of mathematical models describing the non-steady-state behavior of amperometric biosensors, incorporating diffusion limitations, multistep enzymatic reactions, and sensor architecture effects [9–11]. The application of such models is particularly valuable in the early stages of biosensor design, when it is crucial to determine optimal membrane thickness, enzyme loading, and the configuration of the electrochemical transducer.

In this work, we present the development of a procedure for determining and optimizing the parameters of a mathematical model of an amperometric biosensor based on immobilized pyruvate oxidase. A theoretical study was carried out to evaluate the effect of bioselective membrane parameters on the biosensor's sensitivity to pyruvate.

Materials and Methods

Reagents. Pyruvate oxidase from *Aerococcus sp.* (EC 1.2.3.3) with an activity of 54 U/mg (Sigma-Aldrich Chimie, USA) was used for the preparation of bioselective elements of the biosensors. Sodium pyruvate (Sigma-Aldrich Chimie, USA) served as the substrate. Bovine serum albumin (BSA) and glycerol (Sigma-Aldrich Chimie, Germany) were also employed in membrane fabrication. For enzyme immobilization, a photopolymer containing styrylpyridinium groups (PVA-SbQ) was used. Other inorganic compounds applied in this study were of domestic production and of analytical grade purity.

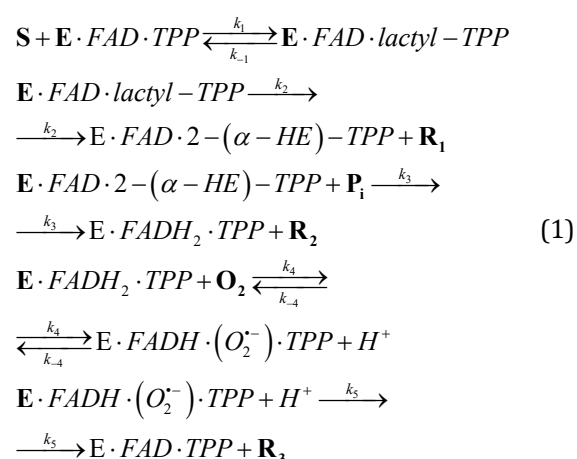Membrane deposition and immobilization procedure. A solution was prepared consisting of 10% POx, 10% BSA, and 3% glycerol. This mixture was combined with a preheated (70 °C) 10% solution of the photopolymer. The resulting solution was deposited on four signal transducers at an average volume of 0.15 μL per sensor. Biosensor exposure was carried out in a Bio-Link BLX-365 chamber under irradiation at 365 nm for 2–10 min with an intensity of 20 J/m².

Measurement procedure. The measurements were performed according to the methodology described in [12]. The biosensors and an *Ag/AgCl* reference electrode (standard single-junction electrode filled with 3 M *KCl*) were connected to a PalmSens potentiostat (Palm Instruments BV, The Netherlands) via a multiplexer from the same manufacturer. Measurements were conducted at room temperature in an open measuring cell with a volume of 1.5 mL, under constant stirring, and at a fixed potential of +0.6 V versus the *Ag/AgCl* reference electrode. A 5 mM phosphate buffer solution (pH 7.4) containing POx cofactors – magnesium ions (125 μM, Mg^{2+}) and thiamine pyrophosphate (*TPP*, 500 μM) – was used as the working buffer. For all experimental studies, sodium pyruvate was added at a final concentration of 0.1 mM.
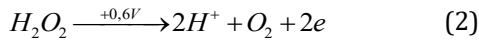
Mathematical modeling and calculations were carried out in the MATLAB environment. The parameter estimation was performed using a custom gradient-descent optimization routine implemented in MATLAB, without relying on built-in solvers. Optimization routine is described in next sections.

Results

The kinetics of the enzymatic reaction involving pyruvate oxidase can be described using the ping-pong mechanism (1):

$$\mathbf{S} + \mathbf{E} \cdot FAD \cdot TPP \underset{k_{-1}}{\overset{k_1}{\rightleftharpoons}} \mathbf{E} \cdot FAD \cdot lactyl - TPP$$

$$\mathbf{E} \cdot FAD \cdot lactyl - TPP \xrightarrow{k_2}$$

$$\xrightarrow{k_2} \mathbf{E} \cdot FAD \cdot 2 - (\alpha - HE) - TPP + \mathbf{R_1}$$

$$\mathbf{E} \cdot FAD \cdot 2 - (\alpha - HE) - TPP + \mathbf{P_i} \xrightarrow{k_3}$$

$$\xrightarrow{k_3} \mathbf{E} \cdot FADH_2 \cdot TPP + \mathbf{R_2}$$

$$\mathbf{E} \cdot FADH_2 \cdot TPP + \mathbf{O_2} \underset{k_{-4}}{\overset{k_4}{\rightleftharpoons}}$$

$$\underset{k_{-4}}{\overset{k_4}{\rightleftharpoons}} \mathbf{E} \cdot FADH \cdot \left(O_2^{\cdot -}\right) \cdot TPP + H^+$$

$$\mathbf{E} \cdot FADH \cdot \left(O_2^{\cdot -}\right) \cdot TPP + H^+ \xrightarrow{k_5}$$

$$\xrightarrow{k_5} \mathbf{E} \cdot FAD \cdot TPP + \mathbf{R_3}$$

(1)

where $\mathbf{E}$ – pyruvate oxidase; $\mathbf{S}$ – pyruvate; $\mathbf{P_i}$ – the corresponding phosphate anion of the multistep reaction; $\mathbf{R_1}$ – carbon monoxide; $\mathbf{R_2}$ – acetyl phosphate; $\mathbf{R_3}$ – hydrogen peroxide. $k_1, k_{-1}, k_2, k_3, k_4, k_{-4}, k_5$ – the rates of the corresponding reactions.

$$H_2O_2 \xrightarrow{+0,6V} 2H^+ + O_2 + 2e \qquad (2)$$

In the case when the phosphate and oxygen concentrations in the buffer are maintained at a constant level and the corresponding constants: $P_i > K_P$ (2.5 > 2.3 mM), $O_2 \gg K_M$ (243 >> 71 μM) and $S \ll K_S$ (0.1 <<9 mM), it is possible to switch from the reaction rate according to the ping-pong mechanism to the enzymatic reaction rate as a pseudo-first-order rate:

$$r = \frac{v_{max}}{K_S / S + K_P / P_i + K_M / O_2 + 1} = \frac{v_{max}^* S}{K_S + S} = kS \quad (3)$$

where is v_{max} – the maximum reaction rate; S, P_i and O_2 are the concentrations of the 1st substrate, the 2nd substrate, and the mediator, respectively; K_S, K_P and K_M are the Michaelis constants for pyruvate, phosphate, and oxygen, respectively.

The transition from the full ping-pong scheme to linear rate in Eq. (3) relies on maintaining phosphate and oxygen in excess, resulting in an effective first-order approximation. Such a linear dependence of the reaction rate on the substrate makes it possible to write a linearized mathematical model in the form of a system of partial differential equations, which in turn has an analytical solution. The mathematical model of the distribution of chemical compounds in the bioselective membrane in this case also loses the trivial equations for the concentrations of phosphate and oxygen (assuming that the diffusion coefficients are close), so the following reaction-diffusion system can be written [10]:

$$\partial_t S = D_S \partial_{xx} S - r$$
$$\partial_t P = D_P \partial_{xx} P + r, \qquad (4)$$
$$x \in (0; L), t > 0$$

where S – pyruvate, P – hydrogen peroxide; D_S and D_P – diffusion coefficients of the substrate and product, respectively; and L – thickness of the protein membrane.

Initial conditions:

$$S(x,0) = S_0(x), \; P(x,0) = P_0(x) \qquad (5)$$

The boundary conditions for both equations can be of either first kind (Neumann) or second kind (Dirichlet); therefore, we employ the general form of third-kind (Robin) boundary conditions, which represent a linear combination of the first two, but with constant coefficients only:

$$a_{S,l} S(0,t) + b_{S,l} \partial_x S(0,t) = c_{S,l}$$
$$a_{S,r} S(L,t) + b_{S,r} \partial_x S(L,t) = c_{S,r}$$
$$a_{P,l} P(0,t) + b_{P,l} \partial_x P(0,t) = c_{P,l} \qquad (6)$$
$$a_{P,r} P(L,t) + b_{P,r} \partial_x P(L,t) = c_{P,r}$$

Next the given values of the coefficients presented in Table 1 will be used in our case.

The solution for each concentration distribution function consists of a solution for the steady-state equation (state) with inhomogeneous boundary conditions (the coefficients $c_{h,g}$ are taken into account) and a solution for the transient part with homogeneous boundary conditions (the Sturm-Liouville problem). Thus, system (4) with conditions (5, 6) has the following general solution:

$$S(x,t) = S_{ss}(x) + \sum_{n=1}^{\infty} A_n^{(S)} X_n(x) e^{-\lambda_n t}$$

$$P(x,t) = P_{ss}(x) + \sum_{m=1}^{\infty} [A_m^{(P)} e^{-\lambda_m t} + \qquad (7)$$

$$\sum_{n=1}^{\infty} \frac{k A_n^{(S)} O_{n,m}}{\| X_m \|^2} E_{n,m}] X_m(x)$$

where $\lambda = \sqrt{k / D_S}$, $\lambda_n = D_S \mu_n^2 + k$, $n = 1, 2..\infty$, $\lambda_m = D_P \mu_m^2$, $m = 1, 2..\infty$.
Modal coupling coefficient:

$$O_{n,m} = \int_0^L X_n(x) \cdot X_m(x) dx \qquad (8)$$

Convolution integral:

$$E_{n,m} = \int_0^t e^{-\lambda_m(t-\tau)} e^{-\lambda_n \tau} d\tau = \frac{e^{-\lambda_m t} - e^{-\lambda_n t}}{\lambda_n - \lambda_m} \qquad (9)$$

The degenerate $\lambda_n = \lambda_m$, when the convolution integral has a solution $-t e^{-\lambda_m t}$ is taken into account, but we will not specifically consider it further.

Table 1: Robin boundary condition coefficients

Indices\variable		a, s⁻¹	b, m/s	c, M/s	Note
1st index	2nd index				
S	l (left boundary)	0	D_S	0	Similar to Neumann condition
	r (right boundary)	-1	D_S	$-S_{bulk}^*$	Robin condition
P	l (left boundary)	1	0	0	Similar to Dirichlet condition
	r (right boundary)	0	D_P	0	Similar to Neumann condition

* S_{bulk} – the concentration of the analyte in the cell, which is equal to the flux value of the analyte through the membrane surface.

Eigenfunctions:

$$X_j(x) = \alpha_j \sin(\mu_j x) + \beta_j \cos(\mu_j x), \; j = n, m \quad (10)$$

The eigenvalues μ_j are found from the equation obtained by substituting the eigenfunctions (10) into the homogeneous boundary conditions:

$$\tanh(\mu_j L) = \frac{a_{j,l} a_{j,r} + b_{j,l} b_{j,r} \mu_j^2}{(a_{j,r} b_{j,l} - a_{j,l} b_{j,r}) \mu_j}, \; j = n, m \quad (11)$$

Solution of homogeneous equations (steady state) for $S_{ss}(x)$ i $P_{ss}(x)$:

$$S_{ss}(x) = A_S e^{\lambda x} + B_S e^{-\lambda x}$$
$$P_{ss}(x) = -D_s / D_P (A_S e^{\lambda x} + B_S e^{-\lambda x}) + C_1 x + C_2 \quad (12)$$

The expressions for the coefficients and integration constants A_s, B_s and C_1, C_2 are found from the system obtained by substituting (12) into the boundary conditions (6).

Modal amplitudes

$$A_n^{(S)} = \frac{1}{\| X_n \|^2} \int_0^L (S_0(x) - S_{ss}(x)) X_n(x) dx \quad (13)$$

$$A_m^{(P)} = \frac{1}{\| X_m \|^2} \int_0^L (P_0(x) - P_{ss}(x)) X_m(x) dx \quad (14)$$

The flow of the product $H_2 O_2$ at the electrode surface ($x = 0$) determines the electric current:

$$I(t) = n_e F A_{tr} D_P \partial_x P(0,t) = G_{ref} D_P \partial_x P(0,t) \quad (15)$$

where $n_e = 2$ – the number of electrons given up by each $H_2 O_2$ molecule, F – the Faraday constant, A_{tr} – the surface area of the electrode.

$$\partial_x P(0,t) = \partial_x P_{ss}(0) + \sum_{m=1}^\infty \alpha_m \mu_m [A_m^{(P)} e^{-\lambda_m t} + \sum_{n=1}^\infty F_{n,m}] \quad (16)$$

with $F_{n,m} = k A_n^{(S)} O_{n,m} E_{n,m} / \| X_m \|^2$

As can be seen, the solution for the hydrogen peroxide concentration (and therefore the biosensor response) depends on the system parameters $I(t) = f(\partial_x P(0,t), k, D_S, D_P, L, a_u, b_v, c_w)$. In this paper, we will consider only the influence of the parameters $W \in \{k, D_S, D_P, L\}$. We can obtain analytical expressions for the sensitivity of the product concentration with respect to each of the parameters. Given that A_s, B_s are equal under our conditions (Table 1), we

have $\partial_x P_{ss}(0) = C_1(W)$.

Biosensor sensitivity with respect to k:

$$\partial_k I(t, W) = G_{ref} D_P (\partial_k C_1 + \sum_{m=1}^\infty \alpha_m \mu_m \times$$
$$\times \sum_{n=1}^\infty [A_n^{(S)} E_{n,m} + k A_n^{(S)} \frac{t e^{-\lambda_n t}(\lambda_n - \lambda_m) - (e^{-\lambda_m t} - e^{-\lambda_n t})}{(\lambda_n - \lambda_m)^2}]) \quad (17)$$

Biosensor sensitivity with respect to D_S:

$$\partial_{D_S} I(t, W) = G_{ref} D_P (\partial_{D_S} C_1 +$$
$$+ \sum_{m=1}^\infty \alpha_m \mu_m \sum_{n=1}^\infty k A_n^{(S)} \mu_n^2 \frac{t e^{-\lambda_n t}(\lambda_n - \lambda_m) - (e^{-\lambda_m t} - e^{-\lambda_n t})}{(\lambda_n - \lambda_m)^2}) \quad (18)$$

Biosensor sensitivity with respect to D_P:

$$\partial_{D_P} I(t, W) = G_{ref} \partial_{D_P} (D_P \partial_x P(0,t)) \quad (19)$$

Biosensor sensitivity with respect to L (resistance):

$$\partial_L I(t, W) = G_{ref} D_P \partial_L (\partial_x P(0,t)) \quad (20)$$

The results of the calculations of the sensitivity of the biosensor relative to the parameters according to formulas (17 – 20) are presented in Fig. 1 – 4. For each sensitivity equation, in addition to the variable parameter, the following constant values were chosen:
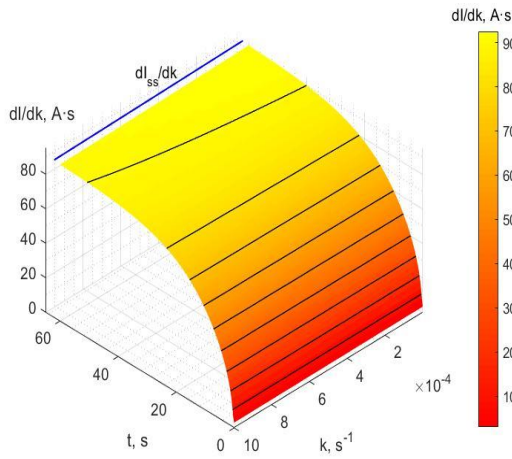$S_0 = 0.1$ mM, $P_0 = 0$, $k = 4.4 \cdot 10^{-10}$ s^{-1}, $D_S = 5 \cdot 10^{-11}$ m^2/s $D_P = 24 \cdot 10^{-10}$ m^2/s, $L = 40$ μm

The steady-state sensitivity curves of the biosensor dI_{ss}/dW are presented in the corresponding Fig. 1 – 4 for each parameter from W for comparison and evaluation. It should be noted that, since the integration constant C_1 depends on all parameters W, the sensitivity of the biosensor will likewise depend on them. For the chosen values of the coefficients from Table 1, in the simplified case:
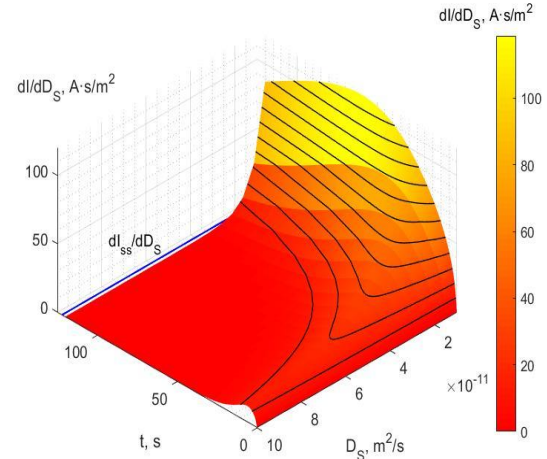
$$A_S = B_S = \frac{c_{s,r}}{2(a_{s,r} \cosh(\lambda L) + b_{s,r} \lambda \sinh(\lambda L))} \approx \frac{c_{s,r}}{2 a_{s,r}} \quad (21)$$

$$C_1 = \frac{2 A_S D_S (a_{p,r} \cosh(\lambda L) + b_{p,r} \lambda \sinh(\lambda L))}{D_P (L a_{p,r} + b_{p,r})} \quad (22)$$
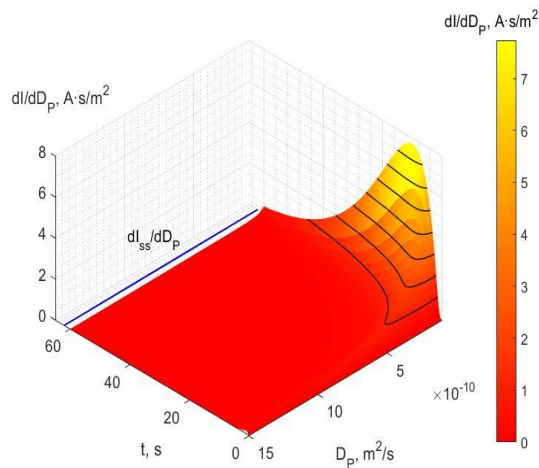
At $t \to \infty$ we have $E_{n,m} = 0$ and $\partial_W E_{n,m} = 0$ therefore only the derivative of the product in the steady state remains, the general formulas for each of biosensor sensitivities with respect to each parameter (while all other parameters remain constant) are presented in Table 2.
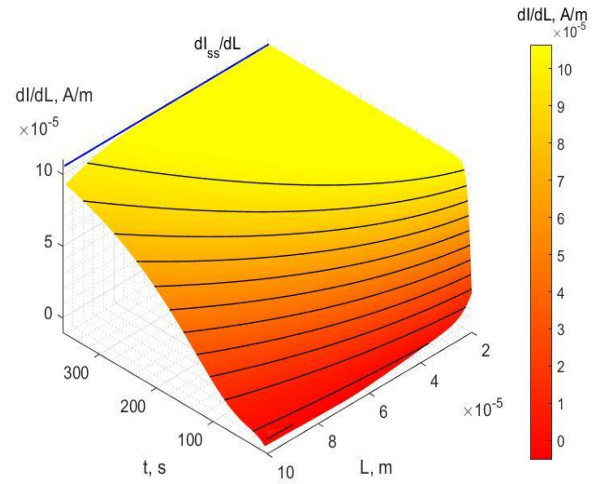
Figure 1: Biosensor sensitivity $\partial_k I(t,k)$ relative to the pseudo-first-order chemical reaction constant k. Isoline step – 10 A·s

Figure 2: Biosensor sensitivity $\partial_{D_S} I(t,D_S)$ relative to the substrate diffusion coefficient – D_S. Isoline step – 10 A·s/m²

Figure 3: Biosensor sensitivity $\partial_{D_P} I(t,D_P)$ relative to the diffusion coefficient – D_P. Isoline step – 1 A·s/m²

Figure 4: Biosensor sensitivity $\partial_L I(t,L)$ relative to membrane thickness – L. Isoline step – 10^{-5} A/m

Table 2: Biosensor sensitivity functions versus system parameters

Parameter (W)	k, s⁻¹	D_S, m²/s	D_P, m²/s	L, m
General formula	$G_{ref} D_P \partial_k C_1(W)$	$G_{ref} D_P \partial_{D_S} C_1(W)$	$G_{ref}(-D_S\lambda(\partial_{D_P}(A_S - B_S)) + C_1(W) + D_P\partial_{D_P}C_1(W))$	$G_{ref} D_P \partial_L(C_1 + \dfrac{(A_S - B_S)k}{\lambda})$
Partial case $\partial_W I_{ss}$	$G_{ref} \dfrac{3S_{bulk}L}{2}$	$G_{ref} \dfrac{S_{bulk}L}{2b_{p,r}} \dfrac{k}{D_S}(\dfrac{b_{s,r}}{a_{s,r}}+1)$	0	$G_{ref} \dfrac{kS_{bulk}}{D_P}(1 + \dfrac{b_{s,r}}{a_{s,r}}\dfrac{1}{L})$
Values of a function	92.52 [A·s]	$19.42 \cdot 10^{-12}/D_S$ [A·s/m²]	0 [A·s/m²]	$10.65 \cdot 10^{-5} \cdot (1 - D_S/L)$ [A/m]

According to the obtained expressions of the partial derivatives of the current (17 – 20) and the current equation (15), all parameters W were optimized simultaneously by the gradient descent method, minimizing the difference:

$$\sum_{i=1}^{N}(I_{\exp}(t_i) - I_{teor}(t_i, W)) \to \min \qquad (23)$$

with the criterion

$$J = \sum_{i=1}^{N}(I_{exp}(t_i) - I_{teor}(t_i))^2 / (2N-1) > \varepsilon \qquad (24)$$

where N is the number of discrete measurements of one experiment, ε is the noise dispersion of experimental data.

The optimization algorithm implemented in MATLAB explicitly computes the analytical sensitivities $\partial_W I(t, W)$ at each iteration and updates all parameters simultaneously using normalized gradient expressions.

For each parameter $W \in \{k, D_S, D_P, L\}$, the update rule was:

$$W_{n+1} = W_n - \frac{\alpha_W}{\|\partial_W I(t)\|}\int_0^T (I_{teor}(t) - I_{\exp}(t))\partial_W I(t)dt \quad (25)$$

which corresponds to a normalized steepest-descent step.

Before main routine of simultaneous optimization, each of parameter in W was exposed to independent optimization with initial conditions of W for 10 steps. Then those intermediate values used in main routine. The algorithm uses same learning rates α_W

for each parameter everywhere. Maximum values $\alpha_W = 0.01$ for each parameter from W was empirically tuned to ensure monotonic reduction of the loss function J. Convergence was reached when either the loss function J dropped below the experimental threshold ε, or when the relative improvement between iterations satisfied:

$$|J_n - J_{n-1}| / J_n < \tau \qquad (26)$$

For all four sensors within a single experiment, the initial parameter values were chosen to be identical. The diffusion coefficients were taken as the standard values for aqueous solutions under normal conditions, while the chemical reaction rate constant was estimated based on the enzyme content in the enzymatic gel with an activity of 5 U/mL. The initial pyruvate concentration was set to $S_{bulk} = 0.1$ mM for all experiments. The total simulation time was 360 s, with the instrument (PalmSens potentiostat) measurement step of 0.3 s. The number of iterations in the algorithm was not less than 400. The results of the optimization process for the biosensor with four sensors are presented in Table 3 and corresponding metrics of results are in Table 4.

Based on the obtained parameter values, theoretical responses were calculated using formula (15). Fig. 5 shows a comparison of experimental data with theoretical current values.
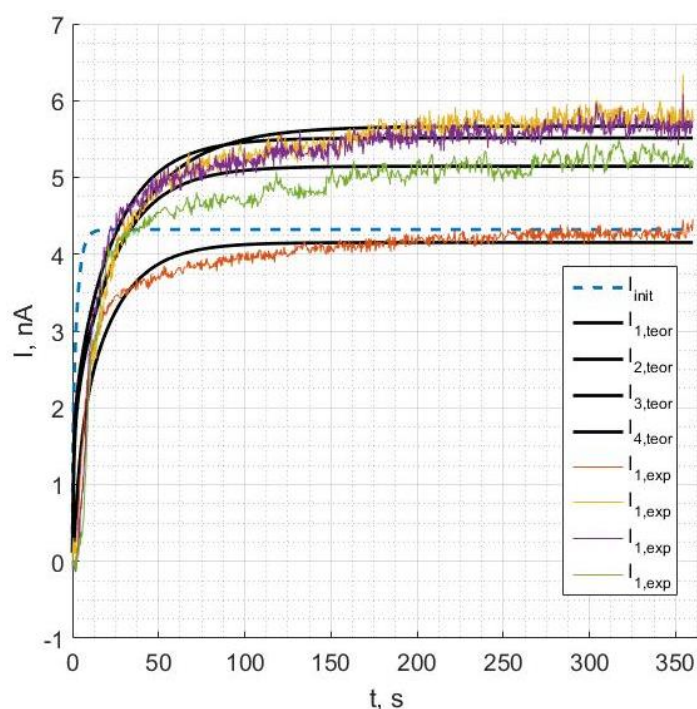
Next we compare experimental responses to 3 pyruvate concentrations (0.1 mM, 0.3 mM and 1 mM) of 4 biosensors with model theoretical values obtained after optimization routine (Fig. 6).
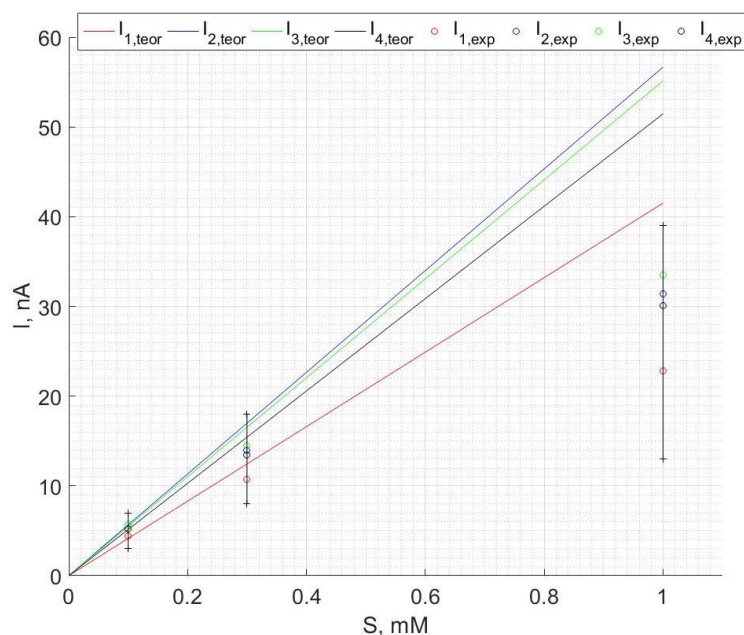
Table 3: Initial and optimal values (mean ± SD)

Optimization routine values	$k \cdot 10^{11}$, s^{-1}	$D_S \cdot 10^{11}$, m²/s	$D_P \cdot 10^{10}$, m²/s	L, µm
Initial values	6	10	25	30
Biosensor № 1	5.6±0.18	1.38±0.16	1.28±0.05	30.9±1.0
Biosensor № 2	7.46 ±0.13	0.95±0.14	0.73±0.06	31.64±0.98
Biosensor № 3	7.51±0.24	1.19±0.12	0.74±0.12	30.58±1.34
Biosensor № 4	7.0±0.19	1.19±0.13	0.63±0.09	30.16±0.96

Table 4: Quantitative metrics of results

Biosensor	R^2	RMSE (A)	MAE (A)	Pearson r
1	0.9341	1.45×10^{-10}	1.16×10^{-10}	0.9665
2	0.9078	2.85×10^{-10}	1.62×10^{-10}	0.9756
3	0.8649	3.18×10^{-10}	1.79×10^{-10}	0.9630
4	0.8223	3.49×10^{-10}	2.11×10^{-10}	0.9506

Figure 5: Comparison of experimental results (4 typical biosensor responses) with the theoretically calculated current (*I*) using the optimized parameters

Figure 6: Comparison of experimental responses with theoretical values of 4 biosensors for different concentrations of pyruvate

Discussion

From the standpoint of study design, this work combines both experimental and theoretical components in a complementary manner. The experimental part focused on obtaining reproducible amperometric responses of pyruvate oxidase – ased biosensors fabricated under controlled conditions, while the theo-retical component aimed to model and predict biosensor performance under various membrane and kinetic parameters. Such a dual design ensured that the mathematical model could be iteratively validated and refined using real experimental data. The decision to study four biosensors fabricated under identical conditions allowed assessment of reproducibility and minimization of random variability between

individual biosensors.

The selection of pyruvate oxidase as the enzymatic element was based on its high substrate specificity and well-characterized reaction mechanism, which simplifies the mathematical description and provides reliable kinetic constants available in the literature. The use of a photopolymer matrix as the immobilization medium was motivated by its favorable diffusion properties, as well as by previous success in enzyme stabilization for long-term biosensor applications. The phosphate buffer composition and the inclusion of essential cofactors (*Mg²⁺* and *TPP*) were taken to maintain consistent enzyme activity during both experimental measurements and model calibration.

Regarding the choice of methods, the amperometric technique was selected for its high sensitivity to hydrogen peroxide – the reaction product of pyruvate oxidase catalysis – which makes it particularly suitable for quantitative kinetic analysis. The reaction–diffusion mathematical model was preferred because it provides an analytical representation of substrate and product concentration profiles across the bioselective membrane. Moreover, the use of the pseudo–first-order approximation was justified for the selected range of pyruvate concentrations ($S \leq 1\,\text{mM}$), where substrate saturation effects are minimal and linearization of the kinetic term significantly simplifies the analysis and optimization procedures. For the calculations and simulations, a minimally sufficient number of modes was employed, $n=m=6$. To verify results calculated from analytical solution for substrate and product (7) we apply to system (4 – 6) MATLAB build in solver pdepe which use method of lines with variable-order numerical differentiation formulas with tolerance $1 \cdot 10^{-6}$. Results of comparison of calculation by these 2 methods actually differ in 6th digit that confirmed expected values from algorithm for analytical solution.

There is known study [13] of ping-pong mechanism for reaction-diffusion system in amperometric biosensor model. The gradient descent optimization algorithm was chosen for its robustness in finding parameter sets that minimize the deviation between theoretical and experimental current responses.

The convergence criteria were chosen based on the physical characteristics of the biosensor system and the numerical properties of the optimization process. The first criterion (24) reflects the fact that the accuracy of the model fit cannot exceed the intrinsic experimental noise level of the amperometric measurement. Once the residual error becomes smaller than the noise amplitudes, further adjustments of the kinetic and diffusion parameters no longer improve the physical fidelity of the model and lead only to numerical overfitting. Therefore, this criterion corresponds to a physically meaningful stopping point: the model reproduces the experimental data as accurately

as actually measurable. The second criterion (26) was introduced to detect the plateau region of the optimization landscape, where successive updates no longer produce a meaningful reduction in the loss function. The threshold value in (26) was selected empirically as the level at which the changes of the loss function fall below both: 1) the numerical precision of the sensitivity integrals and 2) the physical variation caused by sensor-to-sensor fluctuations. A tighter threshold would not affect the final parameters but would significantly increase computation time; a looser threshold ($\tau = 10^{-3} - 10^{-6}$) allows premature termination before parameter stabilization. For $\tau = 10^{-6}$ $400 - 500$ iterations were typically required before satisfying convergence condition (26) or breaking condition (24), and for $\tau = 10^{-5}$ – $90 - 100$ iterations, respectively. Thus, $\tau = 10^{-6}$ provides a balance between computational efficiency and numerical stability.

Together, these two criteria ensure that: 1) the fit does not attempt to model experimental noise and 2) the optimization stops only when further parameter changes are insignificant both numerically and physically.

To reduce the risk of convergence to a local minimum rather than to the global optimum, the optimization was performed with four independent initializations, corresponding to each of the four biosensors fabricated under identical conditions. Because the biosensors are nominally identical but differ slightly enzyme loading, the initial points for gradient descent differ naturally between sensors. Importantly, all four optimization runs converged to similar parameter values (Table 3), indicating the presence of a single dominant global minimum in the parameter landscape for the chosen model. Additional tests with randomized perturbations of initial conditions (±20% variation around the nominal values) yielded the same final parameters within ±5%.

Additional analysis was performed to assess the robustness of the parameter optimization with respect to noise and initial conditions. Introducing ±5% artificial noise resulted in variations of less than 3–7% in the optimized parameters. Perturbing initial parameter guesses by ±20% led to convergence within ±4–6% of the original optimum. The coefficients of variation across the four biosensors were 12.5% (k), 15.4% (D_S), 21.3% (D_P), and 2.9% (L), indicating that the estimation procedure is stable and that the optimized parameters are reproducible. These results confirm that the model reliably identifies physically meaningful parameters under realistic noise and fabrication variability.

Nevertheless, several limitations of the study should be acknowledged. First, the assumption of pseudo–first-order kinetics neglects potential nonlinear effects at higher substrate concentrations, which

may lead to minor discrepancies in the transient phase of biosensor responses. Second, the model assumes uniform enzyme distribution within the membrane and does not explicitly account for enzyme deactivation, leakage, or microheterogeneity of the polymer matrix. Third, the study was conducted under controlled laboratory conditions (constant temperature, stirring, and buffer composition, which may differ from physiological or real-sample environments. These factors could influence the absolute values of diffusion coefficients and reaction rates. Fourth, the correct sensitivity analysis could be done only in small region of parameters near initial values and in our case, we consider upper limit for parameters from W like 10 times of initial values and lower limit as like 0.01 times of initial values according to trends showed on Fig. 1 – 4. Fifth, the linearization of the reaction rate (Eq. 3) imposes a limitation on the substrate concentration S that can be accurately analyzed with this model. Under the linear-rate approximation with $k \approx V_{max}/K_S$, the model overestimates the Michaelis–Menten rate by more than 5% at $S_{LIM} = 0.45$ mM, given the reported $K_S = 9$ mM (results of biosensor responses for comparison on Fig. 6 for $S = 0.3$ mM are still in good agreement with theoretical values).

Comparison of the obtained results with literature data [11, 12, 14 – 16] confirms that the estimated parameters are consistent with values typically reported for oxidase-based enzymatic biosensors. The results from Fig. 5 also comparable with study of amperometric biosensor [15], where response of biosensor on 0.4 mM of pyruvate at room temperatures was in range 4 – 8 nA. In study [16] another biosensor demonstrates responses in the range of tens of nA. Obtained currents by (15) are anodic as expected from (2). Importantly, mathematical modeling allowed us to avoid numerous experimental trials in the development and optimization of the biosensor, since the theoretical response curves showed good agreement with the experimental results. This highlights the potential of the developed approaches for predicting sensor behavior under varying membrane conditions.

By applying a pseudo-first-order kinetic model for the enzymatic conversion rate, analytical solutions and parameter estimations can be obtained. However, the pseudo-first-order kinetic model does not allow accurate evaluation of the transient state of the system, as it does not account for variations in reaction rate associated with enzyme saturation by the substrate (in contrast to the Michaelis–Menten model). As a result, during the initial seconds of the theoretical biosensor response, a linear increase in current is observed, arising both from product accumulation and diffusion.

Thus, at low values of k, the steady-state sensitivity $\partial_k I_{ss}(W)$ remains essentially constant, as observed in Fig. 1 (linear dI_{ss}/dk). The steady-state sensitivity with respect to the substrate diffusion coefficient D_S is inversely proportional to its value; for D_S in the range of $10^{-12} - 10^{-11}$ m²/s, the corresponding slope (dI_{ss}/dD_S) approaches zero. The steady-state sensitivity to the product diffusion coefficient D_P is negligible (Figure 3, line dI_{ss}/dD_P), since $dC_1/dD_P = -C_1/D_P$. The steady-state resistance $\partial_L I_{ss}(W)$ has a constant component and an additional term inversely proportional to the membrane thickness L, while higher-order terms were neglected.

Analysis of Fig. 1 – 4 also allows a deeper assessment of the influence of each key parameter on biosensor operation. As seen in Fig. 1, the biosensor sensitivity with respect to the reaction rate constant k increases linearly over all range of k on 1 A·s at time t=60 s, confirming the critical role of enzymatic activity in shaping the output signal. This means that increasing the amount of active enzyme in the membrane can achieve higher response values; however, there is a limit ($k \gg 10^{-5}$ s⁻¹ and correspondingly $V_{max} \gg 10^{6}$ U), beyond which further increase of enzyme content is ineffective due to diffusion limitations.

Fig. 2 shows the dependence of sensitivity on the substrate diffusion coefficient (D_S). At low D_S values, sensitivity is strongly affected, indicating potential diffusion limitations in thick or dense membranes. For D_S values on the order of 10^{-11} m²/s, the influence becomes less pronounced, and the sensor operates closer to a kinetically controlled regime. Therefore, controlling membrane structure (porosity, hydration) is an important strategy to improve sensor efficiency.

Fig. 3 illustrates that the sensitivity with respect to the product diffusion coefficient (D_P) is effectively zero in the steady state. This observation is consistent with theoretical calculations and indicates that hydrogen peroxide transport from the membrane to the electrode does not constitute a limiting step under the given conditions. Accordingly, optimization efforts should primarily focus on substrate diffusion and the enzymatic reaction rate.

Fig. 4 demonstrates the dependence of sensitivity on membrane thickness (L). With increasing thickness, the response decreases due to increased mass transfer resistance, confirming the critical importance of selecting the sensor's geometric parameters. Optimal performance is achieved using membranes of minimal thickness that still maintain mechanical stability and do not lead to enzyme leakage.

The most convincing confirmation of model adequacy is shown in Fig. 5. Here, the theoretically calculated curves practically coincide with the experimental responses for all four electrodes. This demonstrates that even the simplified assumption of pseudo-first-order kinetics is sufficient to describe system behavior

in the steady state. Some deviations in the transient region are explained by the fact that the model does not account for enzyme saturation by substrate during the first seconds of the reaction, but in the time range above 50 s, the agreement is very high.

Thus, analysis of the graphical results indicates that the mathematical model not only qualitatively describes sensor operation but also enables quantitative predictions necessary for further optimization. This confirms the feasibility of integrating experimental and theoretical approaches in the design of biosensors. Practical novelty lies in obtaining experimentally validated, robustly optimized kinetic and diffusion parameters for POx-based biosensors, enabling rational design decisions without extensive experimental campaigns.

Conclusions

In this work, a procedure for determining and optimizing the parameters of a mathematical model of an amperometric biosensor based on immobilized pyruvate oxidase was developed, aiming to improve the analytical characteristics of the sensor and simplify its development process. The use of a reaction–diffusion mathematical model allowed the optimization of key sensor parameters (k, D_S, D_P, L) and the evaluation of their contribution to the formation of the analytical signal for pyruvate.

The obtained results allow us to make the following generalized conclusions:

The investigated biosensor provides a stable and reproducible amperometric response to pyruvate, as confirmed by the high agreement between theoretical and experimental data.

The determined influence of all parameters on biosensor sensitivity decreases in the following order: from the most influential enzymatic reaction rate constant (k), to the substrate diffusion coefficient (D_S), and then to the membrane thickness (L), while the effect of the product diffusion coefficient (D_P) was minimal.

The membrane thickness is a critical design parameter: excessive increase leads to a significant signal decrease due to mass-transfer limitations. Therefore, a balance must be found between mechanical stability and minimal diffusion resistance.

Mathematical modeling has proven its effectiveness as a tool for prediction and optimization, allowing minimization of the number of experimental measurements and providing a more rational design of the sensor.

In the future, the developed approach can be extended to other biosensors based on different enzymatic systems. Moreover, the strategy proposed in this work, combining experimental and theoretical approaches, opens new opportunities for the development of highly sensitive, selective, and reliable biosensors capable of operating effectively in complex biological environments.

Interests disclosure

Oleksandr Soldatkin is a member of the editorial board of *Innovative Biosystems and Bioengineering* and was not involved in the editorial evaluation or decision-making regarding the publication of this article.

References

[1] Berg, J. M., Tymoczko, J. L., & Stryer, L. (2015). Biochemistry. 8th ed. W.H. Freeman and Company. ISBN 1464126100, 9781464126109

[2] Sutendra G, Michelakis ED. Pyruvate dehydrogenase kinase as a novel therapeutic target in oncology. Frontiers in oncology. 2013 Mar 7; 3:38. DOI: 10.3389/fonc.2013.00038

[3] Lu W, Clasquin MF, Melamud E, Amador-Noguez D, Caudy AA, Rabinowitz JD. Metabolomic Analysis via Reversed-Phase Ion-Pairing Liquid Chromatography Coupled to a Stand Alone Orbitrap Mass Spectrometer. Analytical Chemistry. 2010 Apr 15;82(8):3212–21. DOI: 10.1021/ac902837x

[4] Dzyadevych SV, Arkhypova VN, Soldatkin AP, El'skaya AV, Martelet C, Jaffrezic-Renault N. Amperometric enzyme biosensors: Past, present and future. IRBM [Internet]. 2008 Apr 1 [cited 2020 Apr 11];29(2):171–80. DOI: 10.1016/j.rbmret.2007.11.007

[5] Mizutani F, Soichi Yabuki, Sato Y, Takahiro Sawaguchi, Iijima S. Amperometric determination of pyruvate, phosphate and urea using enzyme electrodes based on pyruvate oxidase-containing poly(vinyl alcohol)/polyion complex-bilayer membrane. Electrochimica acta. 2000 Jun 1;45(18):2945–52. DOI: 10.1016/S0013-4686(00)00373-X

[6] Korkut S, Keskinler B, Erhan E. An amperometric biosensor based on multiwalled carbon nanotube-poly(pyrrole)-horseradish peroxidase nanobiocomposite film for determination of phenol derivatives. Talanta. 2008 Sep 15;76(5):1147–52. DOI: 10.1016/j.talanta.2008.05.016

[7] Piro B, Reisberg S. Recent Advances in Electrochemical Immunosensors. Sensors. 2017 Apr 7;17(4):794. DOI: 10.3390/s17040794

[8] Yakovleva ME, Killyéni A, Ortiz R, Schulz C, MacAodha D, Conghaile PÓ, et al. Recombinant pyranose dehydrogenase —A versatile enzyme possessing both mediated and direct electron transfer. Electrochemistry Communications. 2012 Sep 8;24:120–2. DOI: 10.1016/j.elecom.2012.08.029

[9] Baronas R, Ivanauskas F, Kulys J. Mathematical Modeling of Biosensors. Springer Series on Chemical Sensors and Biosensors. Dordrecht: Springer Netherlands; 2010. Springer eBook ISBN978-90-481-3243-0 DOI: 10.1007/978-90-481-3243-0

[10] Baronas R, Kulys J. Modelling Amperometric Biosensors Based on Chemically Modified Electrodes. Sensors. 2008 Aug 19; 8(8):4800–20. DOI: 10.3390/s8084800

[11] Sierra-Padilla A, García-Guzmán JJ, Blanco-Díaz L, Bellido-Milla D, José María Palacios-Santander, Cubillana-Aguilera L. Innovative Multipolymer-Based Electrochemical Biosensor Built on a Sonogel–Carbon Electrode Aiming for Continuous and Real-Time Lactate Determination in Physiological Samples: A New Scenario to Exploit Additive Printing. Engineering Proceedings. 2023 Sep 26;48(1):48. DOI: 10.3390/CSAC2023-14902

[12] Kucherenko IS, Soldatkin OO, Topolnikova YV, Dzyadevych SV, Soldatkin AP. Novel Multiplexed Biosensor System for the Determination of Lactate and Pyruvate in Blood Serum. Electroanalysis. 2019 May 22;31(8):1608–14. DOI: 10.1002/elan.201900229

[13] Romero MR, Baruzzi AM, Garay F. Mathematical modeling and experimental results of a sandwich-type amperometric biosensor. Sensors and Actuators B: Chemical. 2012 Feb;162(1):284–91. DOI: 10.1016/j.snb.2011.12.079

[14] Jose R, Madalina Maria Barsan, Sanz CG, Diculescu VC. Electrochemical bienzymatic biosensor for pyruvate kinase activity evaluation and inhibitor screening. Talanta. 2025 Mar 1; 291(6):127886. DOI: 10.1016/j.talanta.2025.127886

[15] Malik M, Chaudhary R, Pundir CS. An improved enzyme nanoparticles based amperometric pyruvate biosensor for detection of pyruvate in serum. Enzyme and Microbial Technology. 2019 Jan 11;123:30–8. DOI: 10.1016/j.enzmictec.2019.01.006

[16] Md. Aminur Rahman, Park DS, Chang SC, McNeil CJ, Shim YB. The biosensor based on the pyruvate oxidase modified conducting polymer for phosphate ions determinations. Biosensors & bioelectronics/Biosensors & bioelectronics (Online). 2006 Jan 1;21(7):1116–24. DOI: 10.1016/j.bios.2005.04.008

Ю.В. Карпенко [1*], О.О. Солдаткін [1,2], Н. Жафрезик-Рено [3]

[1]Інститут молекулярної біології та генетики НАН України, Київ, Україна
[2]Київський політехнічний інститут імені Ігоря Сікорського, Київ, Україна
[3]Інститут аналітичних наук, Університет Ліона, Вільюрбан, Франція

ДОСЛІДЖЕННЯ ПАРАМЕТРІВ ТА ОПТИМІЗАЦІЯ АМПЕРОМЕТРИЧНОГО БІОСЕНСОРА ДЛЯ ВИЗНАЧЕННЯ ПІРУВАТУ ЗА ДОПОМОГОЮ МАТЕМАТИЧНОГО МОДЕЛЮВАННЯ

Вступ. Піруват є важливим діагностичним маркером мітохондріальних дисфункцій, лактат-ацидозу та деяких онкологічних захворювань. Традиційні методи аналізу пірувату мають низку суттєвих обмежень: потребують складної апаратури, є трудомісткими, займають значний час підготовки проб. Тому розробка нових, чутливих та селективних методів визначення концентрації пірувату є актуальною задачею.

Мета. Метою роботи було розробити процедуру визначення і оптимізації параметрів математичної моделі амперометричного біосенсора на основі іммобілізованої піруватоксидази із застосуванням математичного моделювання дифузійно-реакційних процесів.

Методи. Біосенсор виготовляли з використанням фотополімерної матриці. Аналітичні характеристики біосенсора досліджували експериментально. Розроблено реакційно-дифузійну математичну модель для аналізу чутливості біосенсора до субстрату (пірувату) відносно параметрів системи. Оптимізація цих параметрів здійснювалася методом градієнтного спуску.

Результати. В роботі було показано, що біосенсор на основі піруват оксидази демонстрував стабільний амперометричний відгук на піруват. Аналіз моделі показав суттєвий вплив коефіцієнту дифузії субстрату та товщини біоселективної мембрани на чутливість біосенсора до пірувату. Відгуки чотирьох біосенсорів відзначались високою відтворюваністю сигналів. Теоретичні, розраховані криві сигналів біосенсора добре узгоджувалися з експериментальними даними.

Висновки. Біосенсор характеризується високою чутливістю та відтворюваністю при визначенні пірувату. Математичне моделювання дозволило здійснити раціональну оптимізацію параметрів даного біосенсора. Визначений вплив усіх параметрів на чутливість біосенсора спадає у такому порядку: від найбільш впливової константи швидкості ферментативної реакції (k), до коефіцієнта дифузії субстрату (D_S) до товщини мембрани (L), тоді як вплив коефіцієнта дифузії продукту (D_P) взагалі був мінімальним.

Ключові слова: піруват; амперометричний біосенсор; піруватоксидаза; реакційно-дифузійна модель; оптимізація